

# A Polarimetric Search for Ice Crystals in the Upper Atmosphere of Venus<sup>1</sup>

G. P. KÖNNEN

*Royal Netherlands Meteorological Institute, P.O. Box 201, 3730 AE De Bilt, the Netherlands*

AND

A. A. SCHOENMAKER AND J. TINBERGEN

*Kapteyn Observatory, Mensingheweg 20, 9301 KA Roden, the Netherlands*

Received July 31, 1992; Revised December 8, 1992

We report a search, at wavelengths between 402 and 850 nm, for anomalies in the Venus polarization curve near the 22° halo scattering angle for ice crystals (phase angle 158°). Such anomalies, if present, can be interpreted as due to halo birefringence peaks. Anomalous polarization was indeed found in the scattering angle range 23–25°, at wavelengths of 622 nm and longer. The largest anomaly was about 0.4% in degree of polarization and occurred at the longest wavelength. The width of the anomaly was 1–3° in scattering angle; both magnitude and width varied with time. Mostly, the anomaly consisted of a dip in polarization (as expected), but one run shows a peak at 622 and 712 nm. One explanation of the dip is halo scattering by H<sub>2</sub>SO<sub>4</sub>-contaminated ice crystals located in the upper haze layer, but the observed deep red color of the anomaly does raise doubts about this mechanism or its completeness. Rapid fluctuations are superposed on the dip; they may be explained by transparency fluctuations due to moving atmospheric features at higher levels. The anomalous peak at 622 and 712 nm requires a separate explanation; it might be due to a transient polarized feature in the upper atmosphere, either overcompensating or obscuring the dip. The physical nature of this feature could not be identified. To separate transient time-dependent effects from scattering-angle effects and to develop polarimetry into an effective remote-sensing tool for birefringent atmospheric constituents, a high-spatial-resolution (spectro-)polarimeter is required, operating from an orbiter. We advocate equipping planetary orbiters with such polarimeters. © 1993 Academic Press, Inc.

## 1. INTRODUCTION

In the late sixties, halo scattering was recognized as a diagnostic for the detection of crystals in planetary atmo-

<sup>1</sup>Based on observations obtained at the Observatorio del Roque de los Muchachos, La Palma, Spain and at the European Southern Observatory (ESO), La Silla, Chile.

spheres (O'Leary 1966). Subsequently, a few attempts were undertaken to detect a Venus H<sub>2</sub>O-ice halo anomaly near a scattering angle of 22° (phase angle 158°), in intensity (O'Leary 1966, 1970, Ward and O'Leary 1972) and in polarization (Veverka 1971). Although the intensity measurement around the 1969 inferior conjunction suggested a marginal increase by 6% (O'Leary 1970), the other observations failed to confirm this. They put an upper limit to the Venus halo anomaly of 5% in intensity (Ward and O'Leary 1972) and of 0.2% in polarization (Veverka 1971). Nevertheless, the atmospheric thermal structure (Seiff *et al.* 1980, Seiff 1983) and composition (Knollenberg *et al.* 1980, Esposito *et al.* 1983) inferred from Pioneer Venus data still do not exclude ice crystals, perhaps contaminated with sulfuric acid, in the upper atmosphere. Information about the presence of such solid particles is needed for a better insight into the atmospheric chemistry and circulation on Venus.

Two factors stimulated us to pick up this thread again. First, observations of terrestrial ice crystal halos (Können and Tinbergen 1991, Können 1992) show that polarimetry is a much more sensitive method for detecting halos from birefringent crystals than previously anticipated; the polarization anomaly produced by the 22° ice halo can be more than five times larger than the previously (Lommel 1877, O'Leary 1966) accepted value. The detectability of a halo anomaly in a high-resolution time series of polarization measurements is further improved by its small width in scattering angle, rarely more than one or two degrees. Second, one of us (J.T.) designed a multichannel polarimeter, the Multi Purpose Fotometer "MPF". With this instrument we expected to obtain the Venus polarization with higher precision and in greater detail than earlier observers (Dollfus and Coffeen 1970, Veverka 1971).

For detection of the halo anomaly in polarization, a

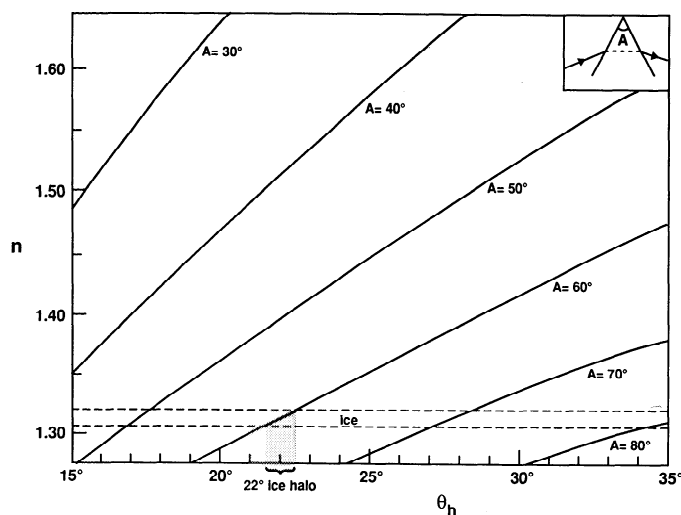


FIG. 1. Halo angles  $\theta_h$  is as a function of the refraction angle  $A$  and the index of refraction  $n$ .

time series of high quality is required. The reasons are the small width of the peak and the fact that the scattering angle changes by  $1.8^\circ/\text{day}$  when Venus is near the halo scattering angle. The time series must extend over several days and almost any day in it is indispensable. At several Venus inferior conjunction years from 1983 to 1988, we made attempts to obtain such a time series. On the last occasion, all 12 channels of the MPF were operational, yielding multiwavelength data with some redundancy and in a near-perfect time series.

In this paper we report the results of our campaigns. Sections 2 and 3 discuss some facts concerning Venus halos and halo polarization. Section 4 presents the techniques of measurement, Section 5 the observational results. The results are discussed and interpreted in Section 6. Section 7 summarizes our conclusions.

## 2. LIGHT DISTRIBUTIONS OF VENUS HALOS

Scattering of light by crystals gives rise to phenomena called halos. The theory and the characteristics of terrestrial ice crystal halos have been extensively discussed in the literature (see e.g., Minnaert 1954, Greenler 1980, Können 1985, Tape, in preparation). An important subset are the refraction halos, arising from light rays which pass through the crystals without internal reflections. For these, the halo angle  $\theta_h$  is given by the well-known minimum deviation formula for a prism:

$$\sin\left(\frac{\theta_h + A}{2}\right) = n \sin\frac{A}{2}, \quad (1)$$

where  $A$  is the angle between the refracting crystal faces and  $n$  the index of refraction. Figure 1 shows the relation

between  $A$ ,  $n$  and  $\theta_h$  for an  $n$ -range covering the refraction index of most transparent substances. Halo angles larger than those depicted in Fig. 1 are possible, but the intensity of very wide angle halos is low. In practice, natural crystals rarely produce refraction halos of significant intensity at scattering angles beyond  $60^\circ$ .

An ice crystal ( $n = 1.31$ ) in its common form is a hexagonal column or plate with flat ends. Its most significant halo angle is  $22^\circ$ , arising from  $A = 60^\circ$ . The light distribution of the resulting halos depends on the preferential orientation of the crystals. The most important cases are the following:

1. Randomly oriented crystals. In the Earth's atmosphere these give rise to a colored circle around the Sun, called "the"  $22^\circ$  halo. If the Venus atmosphere contains such crystals, they will give rise to a halo anomaly in intensity and polarization. This anomaly would show up over the whole crescent, from any place where ice crystals are found. It may be detected when Venus passes through the halo angle (Fig. 2), which happens about 10 days before and after inferior conjunction.

2. Ice crystals with their principal axis (C-axis) preferentially oriented horizontally. On Earth these give rise to what are called the tangent arcs to the  $22^\circ$  halo, at its highest and lowest point. For Venus they would cause a halo signal near places where the Venus gravity vector is in the plane of scattering. Hence, tangent arc scattering from Venus would be visible only near the equatorial portion of the crescent.

3. Ice crystals with the C-axis preferentially vertically oriented. On Earth these generate the parhelia, bright spots located somewhat outside the azimuthal extremes of the  $22^\circ$  halo. For Venus, parheliion scattering would be visible only near the poles of the crescent, where the Venus gravity vector makes a right angle with the scattering plane.

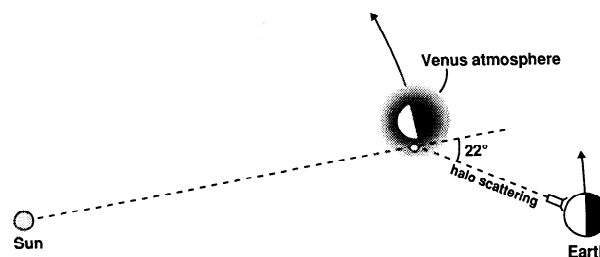


FIG. 2. Halo scattering due to refraction from two prism faces of hexagonal ice may be detected when the Venus scattering angle is around  $22^\circ$ . If the crystals are randomly oriented, halo light may come from the entire Venus crescent. Halo scattering by crystals with a horizontally oriented C-axis (tangent arc scattering) will be visible only near the equatorial part of the Venus crescent. If the C-axis is vertically oriented (parheliion scattering), the halo signal will be located only near the poles of the Venus crescent (not explored in our measurements).

To reach a definite assessment about the presence or absence of a given crystal, at least the three above-mentioned cases have to be investigated. Equator-only observations like ours can only detect crystals in orientation mode 1 or 2 with no information about their relative contribution.

### 3. HALO POLARIZATION

Birefringence of ice crystals results in strong polarization of the inner edge of refraction halos. A general theory of this feature has been published elsewhere (Können and Tinbergen 1991). In this section we apply it to the 22° ice halo. For that halo the optical crystal axis (the C-axis) is parallel to both refracting faces. Hence, the minimum deviation rays (see the insert of Fig. 1) cross the optical axis at a right angle and therefore this axis is perpendicular to the scattering plane if the refracting faces are in minimum deviation configuration. These facts simplify the theory considerably.

The strong polarization arises because the halo consists of two completely polarized components, mutually shifted. The reason is the polarization dependence of  $n$ . Light vibrating parallel to the optical axis is subject to the extraordinary index of refraction  $n_e$ , light vibrating perpendicularly to that axis is subject to the ordinary one,  $n_o$ . For ice,  $n_e - n_o = 0.0014$  (Hobbs 1974) and thus the halo due to ordinary refraction is slightly shifted toward smaller scattering angles (Eq. (1)). Maximum polarization occurs in the region where the intensity of the halo changes fastest with scattering angle. This occurs near the halo angle. The relative shift of the two polarized halo components results in a narrow peak in the halo polarization. This “birefringence peak” of the halo is centered at the polarization-averaged halo angle.

An important parameter for the calculation of the polarization is  $\Delta\theta_h$ , which is the halo angle for polarization perpendicular to the plane of scattering minus that for polarization parallel to it. Its sign depends on the position of the optical axis with respect to the scattering plane and is positive for the 22° halo. This implies that the polarization of the inner 22° halo component and hence that of the birefringence peak is in the plane of scattering. The value of  $\Delta\theta_h$  can be found from the first derivative of Eq. (1), yielding

$$\Delta\theta_h = 76^\circ(n_e - n_o) = 0.11^\circ. \quad (2)$$

$\Delta\theta_h$  shows a slight wavelength dependence. In the range of 400–850 nm,  $n_e - n_o$  varies by 10% (Hobbs 1974) and  $\Delta\theta_h$  behaves accordingly. The temperature dependence of  $\Delta\theta_h$  is very small: at 85 K  $n_e - n_o$  is lower than at melting point by 5.5%, whereas above 170 K  $n_e - n_o$  is constant within 0.4% (Kahane 1962).

In the geometric optical approximation the intensity distribution of halos generated by isotropic crystals and by a point source of light is characterized by a jump from zero to its maximum value at the halo angle. In the birefringent case the maximum is reached in two jumps, occurring at the two respective halo angles. Between these jumps only one of the polarized components is visible, resulting in a steep birefringence peak, of width  $\Delta\theta_h$ . Its intensity and its second Stokes parameter  $Q$  are equal and amount to about half the maximum halo intensity, while its third Stokes parameter  $U$  is zero; the plane of reference of  $(Q, U)$  is the scattering plane. For many halos, including the 22° ice crystal halo, the polarization outside the region of the birefringence peak can be neglected.

In reality both the halo intensity and the birefringence peak are smoothed by the solar disk and by diffraction. The maximum intensity  $I_H$  is still approximately the same as that in geometrical optics, while the second Stokes parameter at the maximum of the birefringence peak  $Q_H$ , becomes (Können and Tinbergen 1991)

$$Q_H = \frac{1}{2\pi} \frac{\Delta\theta_h}{\theta_{1/2}} I_H. \quad (3)$$

Here  $\theta_{1/2}$  is half the FWHM of the smoothing function. Expressed in degrees

$$\theta_{1/2}^2 = \left( \frac{180^\circ}{\pi} \frac{\lambda}{a} \right)^2 + (1/2s)^2. \quad (4)$$

The first term of Eq. (4) represents the effect of diffraction, in which  $\lambda$  is the wavelength and  $a$  is the slitwidth in the cloud of crystals that contributes most to the halo intensity (Können 1992); for 22° halo scattering, the relation between the slitwidth  $a$  and the diameter  $d$  of a hexagonal face of the ice crystal is  $d = 2.6a$ . The second term of Eq. (4) represents solar disk smearing, where  $s$  is the semidiameter of the Sun ( $0.37^\circ$  as seen from Venus). From Eqs. (2)–(4) one finds for a 22° ice halo on Venus that

$$Q_H \leq 0.10 I_H, \quad (5)$$

in which the equal sign refers to very large crystals (zero diffraction).

We consider the Venus degree of polarization  $P$ . Following the usual convention, the degree of polarization is  $P = -Q/I$ , which is negative for polarization in the plane of scattering. A Venus halo will be superposed on a polarized background of intensity  $I_B$  and second Stokes parameter  $Q_B$ . We define the Venus background degree of polarization by  $P_B = Q_B/I_B$ . A Venus halo results in a deviation

of  $P(\theta)$  from  $P_B$  by maximally  $P_H$ ; we shall call  $P_H$  the halo anomaly. From its definition it follows that

$$P_H \equiv P - P_B = -\frac{Q_H}{I_H + I_B} - \frac{Q_B}{I_H + I_B} + \frac{Q_B}{I_B} \equiv -\frac{Q_H}{I_B}, \quad (6)$$

where in the last step the assumption has been made that  $I_H \ll I_B$ . For the  $22^\circ$  halo,  $Q_H > 0$  and hence  $P_H < 0$ . The contribution of the halo to the planetary intensity can be calculated from  $P_H$  by substituting Eqs. (3) and (4) into Eq. (6); its lower limit follows from Eq. (5):

$$I_H/I_B \geq 10 |P_H|. \quad (7)$$

The theory outlined here is formulated explicitly for the  $22^\circ$  ice halo, resulting in simple expressions for Eqs. (2) and (3). In their present form, they cannot be applied straightforwardly to other halos. First, the sign of  $\Delta\theta_h$  can never be determined from Eq. (2), as it depends also on the orientation of the optical axis with respect to the plane of the minimum deviation ray. This may differ for different halos arising from the same crystal. For instance, for the  $46^\circ$  ice halo ( $A = 90^\circ$ ), the optical axis is in the plane of the minimum deviation ray, resulting in  $\Delta\theta_h < 0$ . Hence, the polarization of its birefringent peak is reversed with respect to that of the  $22^\circ$  halo, in spite of the fact that the inner halo component is in both cases the ordinary refracted one. Second, if the optical axis is inclined to the minimum deviation ray, the absolute value of  $\Delta\theta_h$  is smaller than suggested by the analogue of Eq. (2) for the halo under consideration. This is because now the index of refraction acting on the extraordinary ray is not  $n_e$ , but has a value closer to  $n_o$  instead. This situation also applies to the  $46^\circ$  halo. Third, an inclination of the optical axis with respect to the plane of the minimum deviation ray results in a smaller absolute value of  $Q_H$  than that of Eq. (3). For a further discussion of these aspects, we refer the reader to our earlier paper (Können and Tinbergen 1991).

#### 4. OBSERVATIONS

We obtained time series of the linear polarization of the equatorial portion of the Venus crescent around scattering angle  $\theta = 22^\circ$  at five out of a total of six opportunities in the inferior conjunction years 1983, 1985, and 1988 (Table I). The quality of the runs improved with time. In 1983 we used the ESO polarimeter (Behr 1968), mounted on the Dutch 90-cm telescope at La Silla, Chile. The 1985 and 1988 data were obtained at La Palma, using the 1-m Jacobus Kapteyn Telescope equipped with the MPF polarimeter (Unger *et al.* 1988). The experimental procedure was basically the same for all runs:

1. Direct and singly reflected sunlight in the telescope was kept off the primary mirror by various baffles and screens (Können and Tinbergen 1988). The baffling and vignetting geometry was kept identical with respect to the Sun-Venus configuration for the two runs of 1988 by operating the telescope east and west of the pier, respectively. The zero point polarization of the asymmetrically baffled system was determined at night by observing various unpolarized first magnitude stars (Tinbergen 1979). The orientation of the coordinate system of the polarimeter with respect to the telescope frame was determined from observations of standard stars (Hsu and Breger 1982, P.A. Bastiaansen, private communication 1984). In 1988 it was also determined by means of a daytime measurement of the blue sky in the zenith, at solar elevation  $40^\circ$ . This method yielded the same results as the nighttime observations and proved to be much more efficient.

2. The  $\lambda = 850$  nm filter used in the 1988 runs had a bandwidth of 30 nm; all other filters, 10 nm. The ESO polarimeter was a single-wavelength polarimeter. During the 1983 II run, we measured at two wavelengths alternately. The MPF polarimeter is capable of measuring up to 12 wavelengths simultaneously. In 1985, 4 channels were operational; in 1988 we used all 12, for 8 different wavelengths, 4 of them observed twice for redundancy.

3. The Venus crescent at the  $22^\circ$  halo angle configuration has a diameter of about 1 arcmin; its thickness is only 2 arcsec. The observation geometry is given in the insert of Fig. 3. In the 10-arcsec diaphragm, projection ensures that an area of about  $2000 \times 2500$  km<sup>2</sup> was covered on Venus. The sky background intensity in the 10-arcsec diaphragm was 0.5 to 0.1 times that of Venus, while the polarizations were both of order 1%. Some diffusely scattered sunlight in the dome caused background signal too, its intensity and polarization depending on the dome position. Therefore each Venus observation was bracketed between two sky observations under strictly identical conditions.

4. The observing procedure was: move dome and observe sky and Venus alternately. The sky signal was taken at a distance of 1.5 arcmin at right angles to the direction of the Sun. After four sky and Venus observations and a final sky observation, the dome was moved again. Individual observations took about 2 minutes. The Stokes parameters  $I$ ,  $Q$ ,  $U$  of the sky (in the instrumental coordinate system) were interpolated and subtracted from those observed on Venus. Subsequently,  $Q/I$  and  $U/I$  were calculated, corrected for the system zero-point polarization, and expressed with respect to the scattering plane. The four individual observations were then averaged to yield one point of  $-Q/I$  or  $U/I$  in our figures, corresponding to a time resolution of about 20 minutes and hence a resolution of 1.5 arcmin in scattering angle. Near sunset we

TABLE I  
The Venus Polarization Runs

Run	Before/after inferior conjunction	Dates	Number of days	Range in scattering angle	Location, polarimeter	Number of wavelengths	Remarks
1983 I	Before	14/8–16/8	3	20.9–24.2	La Silla, Behr	1 (440 nm)	Only one point on 14/8
1983 II	After	1/9–3/9	3	19.8–23.6	La Silla, Behr	2 (440, 620 nm)	
1985	After	13/4–15/4	3	22.3–26.3	La Palma, MPF	4 (440–790 nm)	No measurements on the scheduled dates 11/4, 12/4
1988 I	Before	28/5–4/6	7	18.1–31.9	La Palma, MPF	8 (402–850 nm)	No measurements on 3/6
1988 II	After	21/6–26/6	6	18.9–29.1	La Palma, MPF	8 (402–850 nm)	

used twice the number of points with half the observing time each, to ensure proper interpolation of the rapidly decreasing sky signal.

5. Each individual observation above consisted of 10 integrations of 5.4 sec each. Each integration is one complete linear polarimetric measurement at the most basic level; each such measurement involves a least-squares solution for a sinusoid (polarized flux) and an offset (unpolarized flux). This multilevel combination of basic measurements gives ample opportunity to monitor the consistency of errors at these different levels. The optical polarization modulation which gives rise to the sinusoid is at a frequency of 100 Hz.

Table II gives the status of the MPF polarimeter during the two 1988 runs. The standard deviation in polarization represents the value for one point, calculated from the four individual observations of  $Q/I$  and  $U/I$ . For the four longest wavelengths it is close to that expected from photon statistics. For the shorter wavelengths, however, it is increasingly determined by the fluctuating sky intensity.

Figure 3 shows the  $\lambda = 791$  nm results of run 1988 II for both  $-Q/I$  and  $U/I$ . The  $-Q/I$  measurements vary smoothly with  $\theta$ , with a dip near  $\theta = 23^\circ$ ; the  $U/I$  points do not differ significantly from zero, as is typical for all our measurements. The absence of any visible  $U/I$  anomaly in the range of the  $-Q/I$  dip implies that the polarization angle is not affected by the dip, within the precision of the measurements. From now on we shall focus on the measurements of the second Stokes parameter and express the results in  $P = -Q/I$ .

## 5. RESULTS AND ANALYSIS

Figures 4–11 show, separately for each wavelength, the combined results of the 1988 runs. Also shown in each figure is a fourth-order polynomial fit to all points outside  $\theta = 22$ – $26^\circ$ . These curves can be considered an approximation to the Venus polarization in the absence of anomalies. We note:

1. Outside the scattering range  $21$ – $26^\circ$ , the points of the

TABLE II  
Polarimeter Specifications (1988 Runs)

Wavelength/ FWHM bandwidth (nm)	No. of channels used	Calculated <sup>a</sup> halo angle	Standard deviation <sup>b</sup> in $P \times 10^4$	$(P_x)_{\text{zero}} \times 10^4$	$(P_y)_{\text{zero}}^c \times 10^4$
402/10	1	22.56°	8	23 ± 2	-3 ± 2
441/10	2	22.32°	5	23 ± 3	6 ± 3
481/10	2	22.13°	5	26 ± 2	8 ± 4
542/10	1	21.91°	10	41 ± 6	1 ± 6
622/10	2	21.71°	5	6 ± 2	8 ± 2
712/10	1	21.55°	3	-7 ± 2	0 ± 2
791/10	2	21.43°	3	-3 ± 2	4 ± 2
850/30	1	21.35°	6	4 ± 3	-11 ± 3

<sup>a</sup> For temperature  $-3^\circ\text{C}$  and averaged over polarization.

<sup>b</sup> Where two channels were used, the better of the channels is quoted here.

<sup>c</sup>  $(P_x)_{\text{zero}}$  and  $(P_y)_{\text{zero}}$  are the system zero point polarization in the equatorial system.

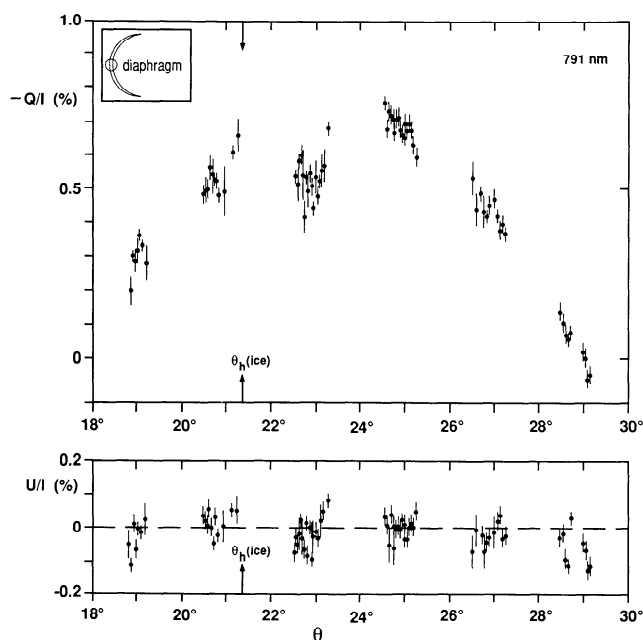


FIG. 3. Polarization of Venus as a function of scattering angle  $\theta$ , measured at wavelength  $\lambda = 791$  nm during run 1988 II (after inferior conjunction). We plot  $-Q/I$ ,  $U/I$  where  $Q$  and  $U$  are the second and third Stokes parameter with the scattering plane as the plane of reference;  $I$  is the intensity.  $\theta_h(\text{ice})$  is the  $22^\circ$  halo angle for pure ice. The  $-Q/I$  curve shows a dip which may be attributed to halo scattering by contaminated ice. Each group of points corresponds to the measurements of 1 day. During the gaps between them, Venus was below the horizon. The insert shows the geometry of observing.

two runs reproduce very well. This holds particularly for the longer wavelengths. The reproducibility of the  $\theta \cong 21^\circ$  points remains an open question due to lack of 1988 I data.

2. In the  $22\text{--}26^\circ$  range, there is anomalous polarization at the four longest wavelengths.

3. If one considers only the 1988 II points (the solid circles), an anomalous dip in the polarization is apparent near  $\theta = 23^\circ$  for  $\lambda = 622\text{--}850$  nm. In the points of that date, the scatter is relatively large.

4. A similar dip is visible in the 1988 I points (open circles) for  $\lambda = 791$  and  $850$  nm. However, the dip is broader: the  $\theta \cong 24.5^\circ$  points are also low. The measurements suggest a sharp rise in the 1988 I polarization between  $\theta = 25^\circ$  and  $\theta = 26^\circ$ .

5. In the 1988 I measurements of  $\lambda = 712$  nm, no dip is apparent at  $\theta \cong 23^\circ$ . If anything, the measurements suggest a peak. Near  $\theta = 24.5^\circ$  the 1988 I polarization decreases rapidly with scattering angle, crossing the interpolated background within the 10 hours of 1 day's observing.

6. In the 1988 I data for  $\lambda = 622$  nm, the polarization near  $\theta = 23^\circ$  is clearly peaked with respect to the remainder of the scan. Near  $\theta = 24.5^\circ$ , the 1988 I polarization drops sharply back to the line representing the background.

7. In the measurements at  $\lambda = 402\text{--}542$  nm, there are no clear anomalies.

If one considers exclusively the 1988 II points, the observational conclusion from the figures could be rather straightforward. The four longest wavelengths consistently show a dip in the polarization near  $\theta \cong 23^\circ$ , becoming more and more pronounced toward the infrared. In the points of the subsequent day,  $\theta \cong 25^\circ$ , the polarization is close to the interpolated background curve, suggesting that the width of the dip is less than  $2^\circ$ .

To estimate the magnitude of this anomaly, Fig. 12 gives the difference in polarization  $\Delta P$  between the daily averaged 1988 II observations and the interpolated background (dashed lines in Figs. 4–11) for the two observation days with  $\theta$  in the  $22\text{--}26^\circ$  range.  $\Delta P$  is represented here as a function of  $\theta - \theta_h(\text{ice})$  rather than as a function of  $\lambda$ , where  $\theta_h(\text{ice})$  is the  $22^\circ$  halo angle for pure ice. For all points of a day the mean  $\theta$  is obviously the same and the variation  $\theta - \theta_h(\text{ice})$  with wavelength comes in by the wavelength dependence of the halo angle (Eq. (1)). A  $(\Delta P, \theta - \theta_h(\text{ice}))$  plot is a diagnostic for halo scattering under singly scattering conditions. If the anomaly is due to halo scattering and there is no strong wavelength-dependent loss of light in its path through the Venus atmosphere or through the crystals, a peak would be apparent in Fig. 12

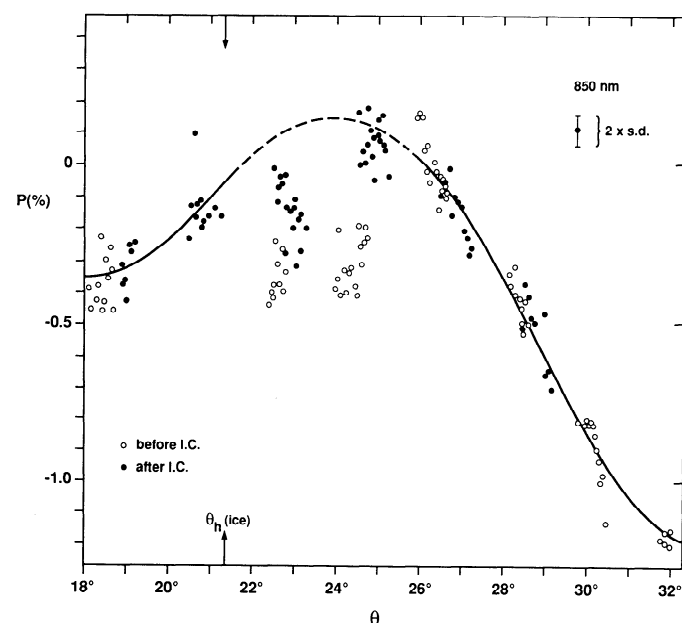


FIG. 4. Degree of polarization  $P(= -Q/I)$  of Venus at  $\lambda = 850$  nm as a function of scattering angle  $\theta$ , measured in 1988. Open circles are before inferior conjunction (1988 I), solid circles after inferior conjunction (1988 II).  $P > 0$  corresponds to polarization perpendicular to the scattering plane. The standard deviation of the points is indicated separately.  $\theta_h(\text{ice})$  is the  $22^\circ$  ice crystal halo angle. The curve is a fourth-order polynomial fit to all points excluding those in the dashed part of the curve.

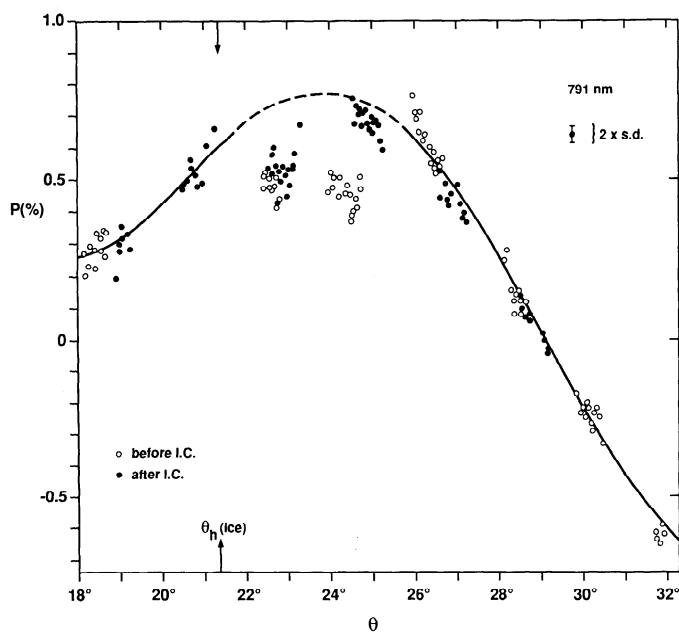


FIG. 5. As Fig. 4, for  $\lambda = 791$  nm. The solid circles are the  $-Q/I$  points of Fig. 3.

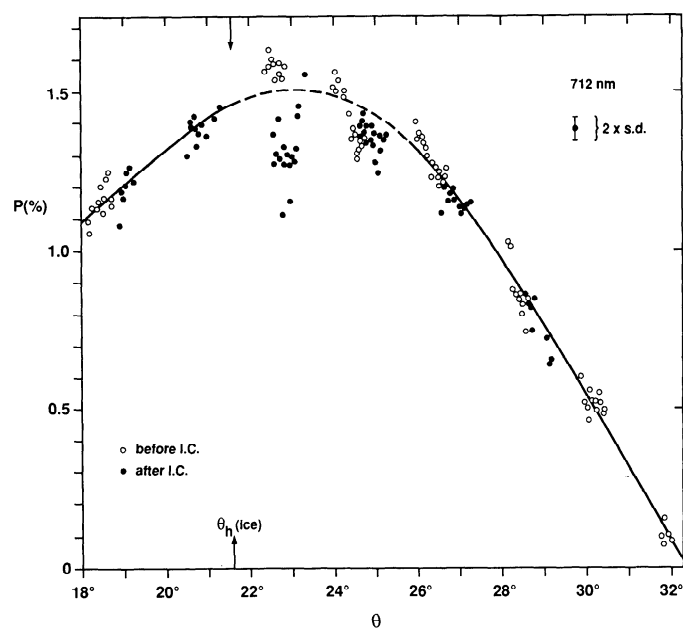


FIG. 6. As Fig. 4, for  $\lambda = 712$  nm.

of a similar sharpness to that of the dips in the  $(P, \theta)$  plots (Figs. 4–11). This holds also for our situation, where the dips are narrow and the wavelength dependence of  $\theta_h$  may have caused them to shift for short wavelengths toward the gaps in the  $(P, \theta)$  plots (Venus below the horizon). However, it is clear from Fig. 12 that the dependence of

$\Delta P$  on  $\theta - \theta_h(\text{ice})$  in no way reflects the shape of the anomalies in the  $(P, \theta)$  plots, Figs. 4–7. Instead, although  $\Delta P$  has been smoothed by the daily averaging procedure, its 23 June points in Fig. 12 show a very steep increase. Since a selection effect due to the gaps is eliminated in this representation, this implies that the strong wavelength

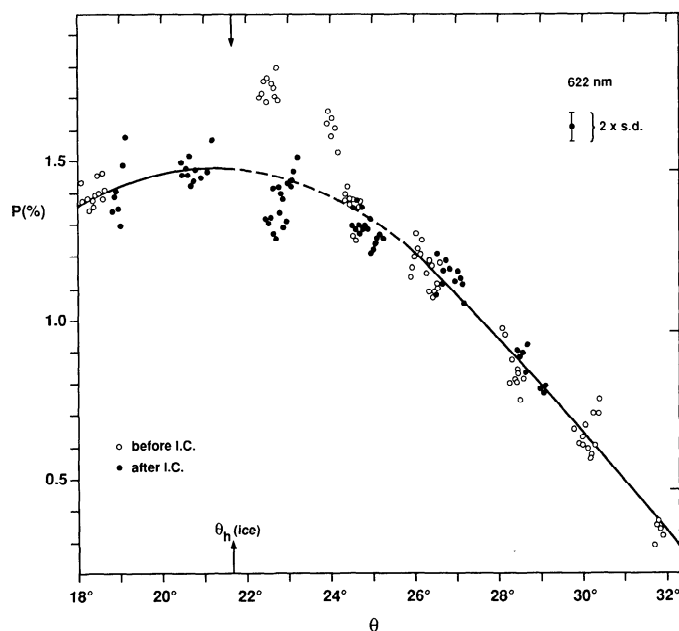


FIG. 7. As Fig. 4, for  $\lambda = 622$  nm.

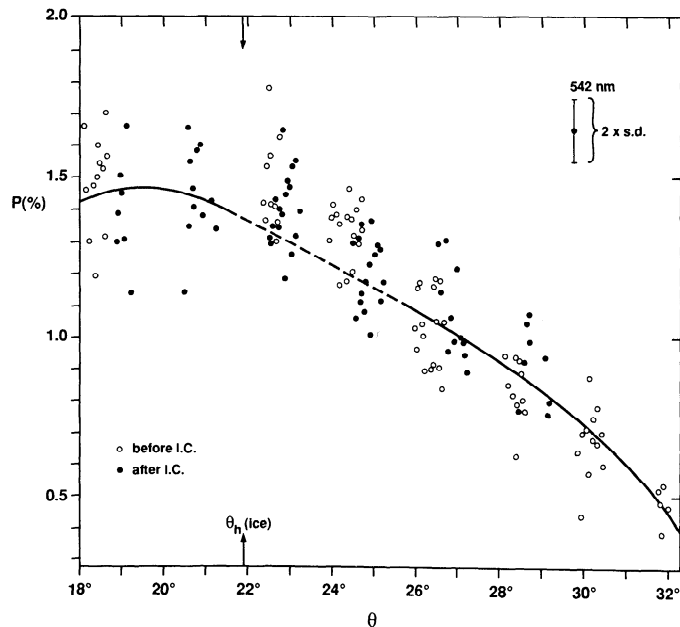
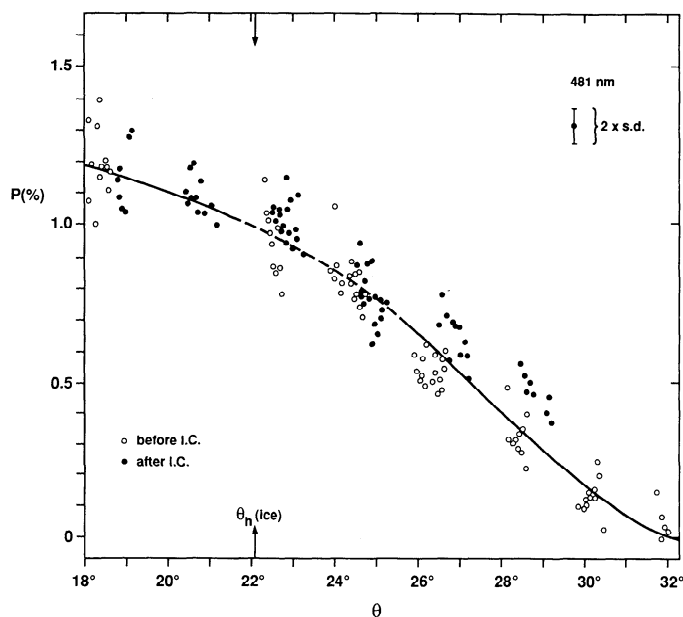
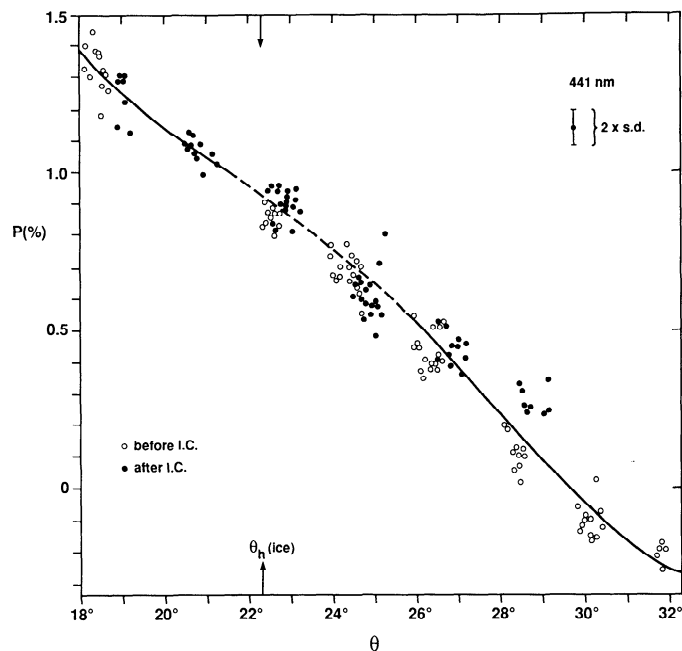


FIG. 8. As Fig. 4, for  $\lambda = 542$  nm.

FIG. 9. As Fig. 4, for  $\lambda = 481$  nm.FIG. 10. As Fig. 4, for  $\lambda = 441$  nm.

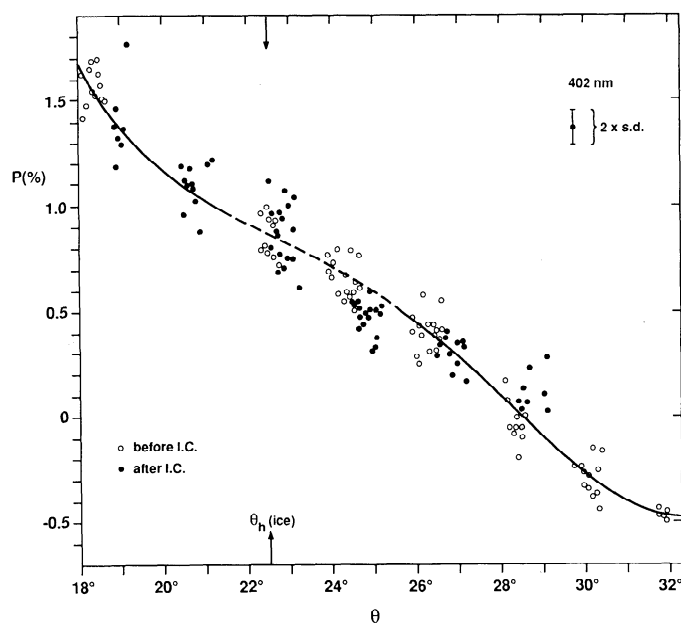
dependence of the magnitude of the anomaly is an intrinsic property.

The magnitude of the anomaly  $\Delta P$  in Fig. 12 ranges up to 0.3%. However, there are reasons to assume that the actual value is higher. First, the background polarizations on which the values of  $\Delta P$  are based, are calculated as fourth-order polynomials producing rather smooth max-

ima. In cases where the anomaly is close to such a maximum, i.e.  $\lambda = 622$ –850 nm, this may underestimate the background polarization and hence the magnitude of  $\Delta P$ , being background minus observed polarization. Indeed, although the open circles in Figs. 4–7 also have been used for calculating the background curves, these observations are near  $\theta = 26^\circ$  significantly above the background curves. Second, in fitting the curves, we also used the  $\theta \cong 21^\circ$  points, but it is possible that these are affected by the anomaly; the absence of data of 1988 I near  $\theta = 21^\circ$  prevents a check of this possibility.

The simple picture of 1988 II—a wavelength-dependent dip, manifesting itself almost exclusively near  $\theta = 23^\circ$ —is complicated significantly when one considers the 1988 I measurements, (remarks 4–6 above). At 850 and 791 nm there is a dip, more pronounced and much broader than in 1988 II. It manifests itself in two subsequent observing days. The  $\Delta P$  plot for 1988 I, Fig. 13, indicates that the anomaly at these wavelengths is about equally strong for both days. For both days, the magnitude of the dip decreases in a similar way with decreasing wavelength; this decrease is even more rapid than in 1988 II. Already at 712 nm there is no dip left, the measurements at  $\theta \cong 23^\circ$  (left part of Fig. 13) suggesting a peak ( $\Delta P < 0$ ) instead. This reversed anomaly becomes very pronounced for  $\lambda = 622$  nm, in both Figs. 7 and 13. We note that 622 nm was a doubly observed wavelength (Table II) and that the results of the two MPF channels are indistinguishable. A hint of behavior analogous to that of  $\lambda = 712$  and 622 nm is apparent in the 542-nm data too.

Part of the reversed anomaly may be caused by the

FIG. 11. As Fig. 4, for  $\lambda = 402$  nm. The vertical scale has been compressed with respect to Figs. 4–10.

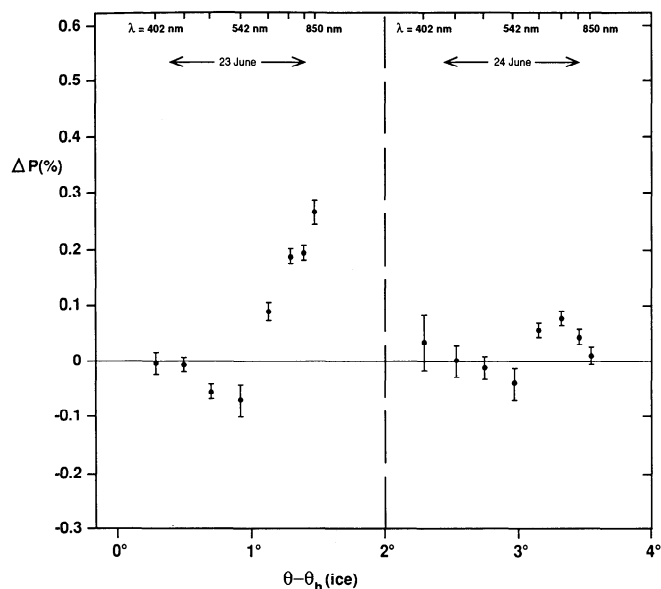


FIG. 12. Daily averages of observed polarization anomaly  $\Delta P$  for each of the eight wavelengths, for the period 1988 II (solid circles in Figs. 4–11).  $\Delta P$  is the difference between the background polarization obtained by interpolation (dashed lines in Figs. 4–11) and the observations.  $\Delta P > 0$  corresponds to a dip with respect to the background curves in Figs. 4–11. The mean scattering angle was  $22.8^\circ$  (June 23rd) and  $24.9^\circ$  (June 24th).  $\theta_h(\text{ice})$  is the  $22^\circ$  halo angle for pure ice, which depends on wavelength. The wavelength  $\lambda$  to which each point refers is indicated at the top of the figure.

above-mentioned underestimate of the background polarization, but we cannot explain it away. Apparently, the dips in the 791–850 nm measurements are in 1988 I indeed accompanied by a peak of similar magnitude and width at  $\lambda = 622$  nm with a sharp cutoff near  $\theta = 24.5^\circ$ .

The 1988 polarization measurements represent a dense covering of points in a rarely observed scattering angle range. Such data may be useful for testing multiple scattering models of the Venus atmosphere. The best representation of the scattering by the atmospheric particles (excluding the anomalous polarization) is given by the curves of Figs. 4 to 11 and the constants of these polynomial fits in Table III. For visible wavelengths, the measurements compare well with earlier observations near the Venus equator (Dollfus and Coffeen 1970, Veverka 1971), but in the infrared (850 nm) our observations are higher by about 2%. Unfortunately, no comparison is possible with Pioneer Venus (Kawabata *et al.* 1980) for lack of sufficient equatorial data in the scattering angle range considered here.

The results of our earlier runs are displayed in Figs. 14 and 15. As they consist of time series of 3 days only, we could not use the interpolation technique for obtaining the background and we compare the results with the background curves of the 1988 data. It is clear that the Venus

polarization varies considerably on a time scale of years (cf. Esposito *et al.* 1983, Hansen and Hovenier 1974), resulting for instance in a change of sign at  $\lambda = 790$  nm. Because of this long-term variability, it is difficult to detect small anomalies in the present plots. However, the longest wavelength of the 1985 data does indicate a decreased and, moreover, a sharply varying polarization near  $\theta = 23^\circ$ . Such an increased variability is also apparent in the points of the 1988 dips, but the variations in the 1985 signal are much more pronounced. They manifest themselves also in the relatively large internal standard deviation of the individual observations contained within one plotted point. There is no reason to suspect the condition of the instrument or the experimental procedure for this one wavelength for this day only, so that these features seem to reflect true rapid fluctuations in the Venus polarization at that wavelength.

We wish to stress that the observational data (particularly for 1988) are quite beyond all reasonable doubt, in spite of the observational handicap of working in the daytime, close to the Sun. The telescope baffling configuration and experimental procedure remained unchanged throughout both series, the equipment by all tests and checks performed well, the highest precision reached was that of photon limits, redundant channels gave identical results and, finally, the polarization angle was as expected. We therefore claim to provide absolutely reliable evidence that the anomalous polarization observed close to the halo angle represents a real effect.

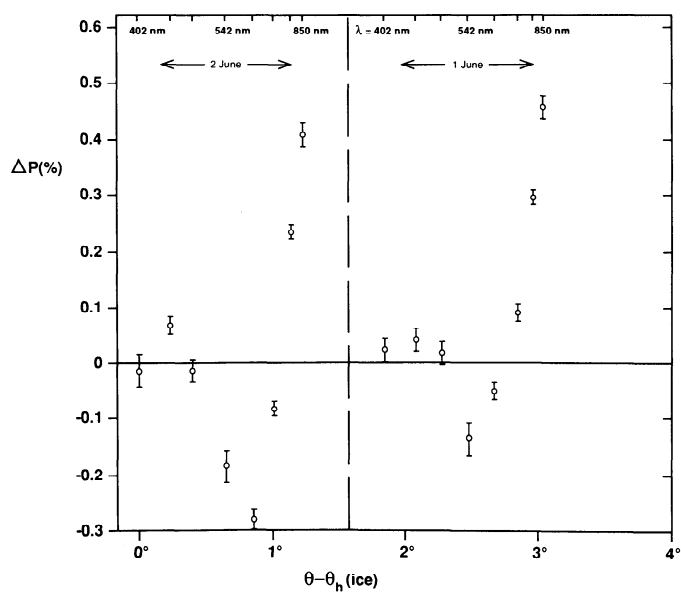


FIG. 13. As Fig. 12, but for the period 1988 I (open circles in Figs. 4–11). Mean scattering angle was  $22.5^\circ$  (June 2nd) and  $24.5^\circ$  (June 1st).

TABLE III  
Background Polarization Summary

Wavelength (nm)	$C_0$	$C_1$	$C_2$	$C_3$	$C_4$
402	+59 ± 3	-13.3 ± 0.9	-1.2 ± 0.3	-0.04 ± 0.03	+0.024 ± 0.006
441	+65 ± 2	-12.1 ± 0.7	-0.7 ± 0.2	+0.01 ± 0.02	+0.010 ± 0.005
481	+76 ± 3	-10.2 ± 0.9	-0.7 ± 0.3	+0.04 ± 0.03	+0.007 ± 0.005
542	+116 ± 3	-7.7 ± 1.0	-0.1 ± 0.3	+0.01 ± 0.03	-0.008 ± 0.006
622	+131 ± 2	-8.8 ± 0.5	-1.2 ± 0.1	+0.03 ± 0.01	+0.004 ± 0.003
712	+142 ± 1	-8.5 ± 0.4	-2.3 ± 0.1	+0.02 ± 0.01	+0.011 ± 0.002
791	+72 ± 1	-7.1 ± 0.3	-3.1 ± 0.1	+0.02 ± 0.01	+0.027 ± 0.002
850	+11 ± 2	-6.5 ± 0.6	-3.4 ± 0.2	+0.01 ± 0.02	+0.033 ± 0.004

Note. Constants used in polynomial fits (curves in Figs. 4–11). The degree of polarization  $P$  as a function of scattering angle  $\theta$  is  $P = 10^{-4} [C_0 + C_1(\theta - 25^\circ) + C_2(\theta - 25^\circ)^2 + C_3(\theta - 25^\circ)^3 + C_4(\theta - 25^\circ)^4]$ .

## 6. DISCUSSION

Both sets of 1988 data show evidence of anomalous polarization in the 22–25° scattering angular range, but only in the longer wavelengths of 622–850 nm. In the 1988 II time series, the anomaly shows up in a narrow range of scattering angle, centered near  $\theta = 23^\circ$ , and has a sign consistent with that expected from a 22° ice halo. At scattering angles between 22.4° and 24.8°, the 1988 I time series taken 3 weeks earlier contains a similar anomaly at the two longest wavelengths, but at 622 and 712 nm it shows an anomaly of the opposite sign, i.e., contrary to that expected from a 22° ice halo. A feature similar to that in 1988 II, though superposed on a background of a different strength, is apparent in the 1985 data.

Although the anomalies are observed only in a narrow scattering angle range, they cannot be unambiguously explained by a well-defined physical process like halo scattering. One reason is the occurrence of anomalies of opposite sign, suggesting that two independent mechanisms are active. A further and more serious complicating factor is that the Venus optical properties depend on the state of its atmosphere, which is changing continuously. Even when a dip recurs in different runs, it is not clear to what extent its shape is determined by change of scattering angle or alternatively by accidental fluctuations in opacity which affect the visibility of the process generating the anomaly. Changes of atmospheric state due to random meteorology can cause differences in the appearance of an anomaly in different runs, but for observations on different sides of Venus there may also be a systematic difference of unknown strength due to atmospheric features locked to the morning (1988 I) and evening terminator (1985, 1988 II); see Knollenberg *et al.* (1980). For a feature showing up in one run only, like the reversed 622-nm anomaly, it remains undecided whether it originated

from some process depending on scattering angle or just from a temporary meteorological quirk.

Leaving this aside for the moment, what would be the consequences of an explanation in terms of halo scattering? The type of the 1988 II anomaly (a dip) is in agreement with that of the 22° ice halo (Eqs. (3) and (6)), its small angular width (<2°) agrees with that observed for terrestrial halos (Können and Tinbergen 1991) and the feature recurs in different runs. However, its scattering angle is about 1.5° higher than that expected from halo scattering by pure ice (see Fig. 12). Equation (2) implies that this requires a shift of +0.02 in the index of refraction; see also Fig. 1. Temperature effects are too small to account for this (Hobbs 1974, Können and Tinbergen 1991). An explanation for this shift could be contamination of the ice crystals by H<sub>2</sub>SO<sub>4</sub>, which is known to be highly abundant in the Venus cloud droplets (Young 1973, Hansen and Hovenier 1974, Knollenberg *et al.* 1980, Knollenberg and Hunten 1980, Esposito *et al.* 1983). An ice–H<sub>2</sub>SO<sub>4</sub> mixture with 12% weight percentage H<sub>2</sub>SO<sub>4</sub> produces the correct index of refraction for the dip (Martens 1906). This corresponds to 1 molecule of H<sub>2</sub>SO<sub>4</sub> in 40 molecules of ice. Such mixtures have melting points well above the highest temperature in the atmospheric column above the cloud tops of 240 K and they have been shown to be stable with respect to splitting out ice (Giauque *et al.* 1960, Ohtake 1993). No details about the optical properties of these crystals are known; a laboratory investigation of ice–H<sub>2</sub>SO<sub>4</sub> mixtures is needed to see whether the birefringence remains large enough to produce a halo polarization anomaly of significant magnitude. We note that the mixture we consider is truly contaminated ice rather than hydrated acid: the highest sulfuric acid hydrate observed in the laboratory is H<sub>2</sub>SO<sub>4</sub>·8H<sub>2</sub>O (Giauque *et al.* 1960).

Terrestrial halos are of a transient nature and the upper Venus atmosphere is dynamic enough to expect a similar

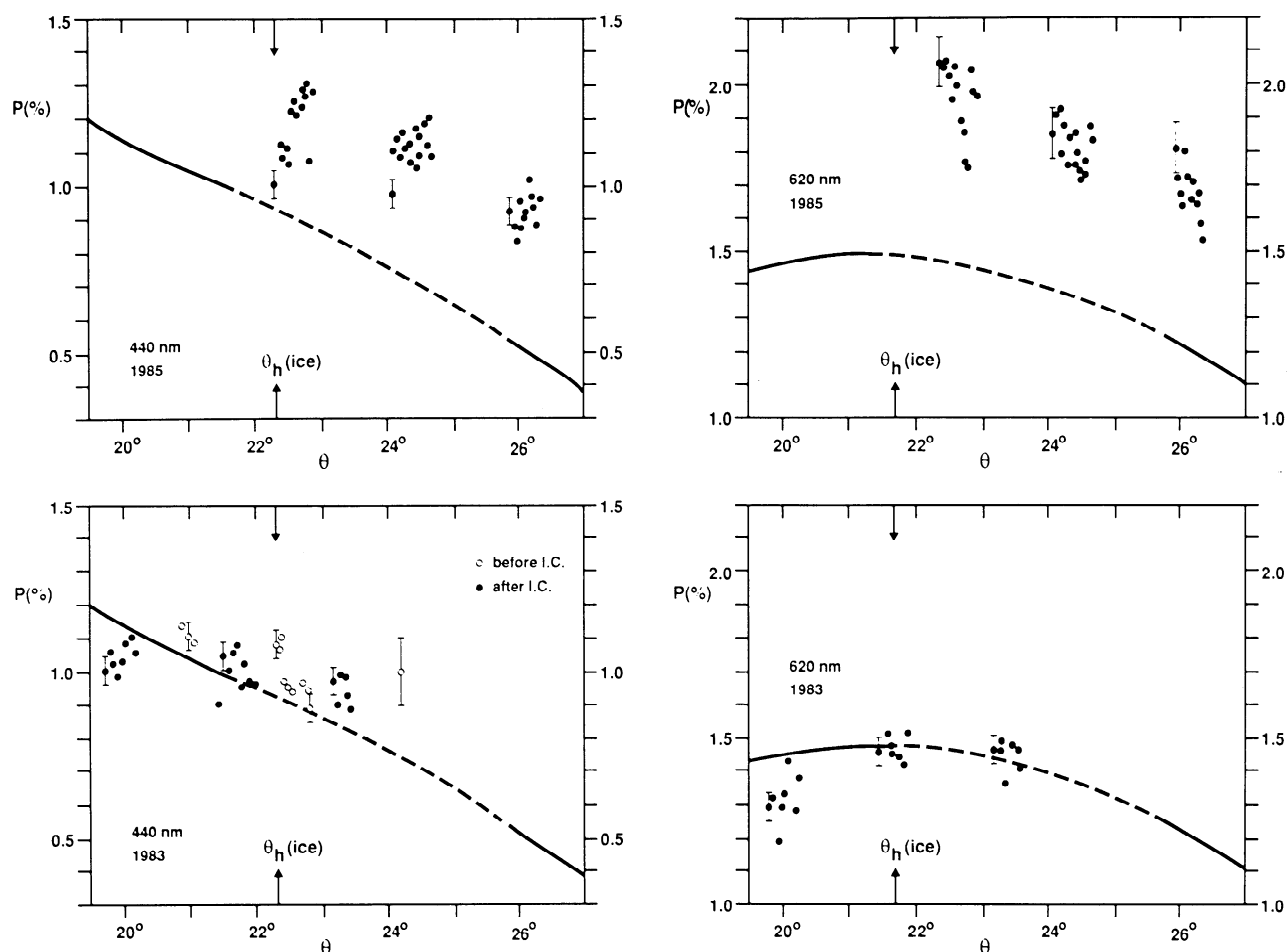


FIG. 14. Venus polarization  $P$  as a function of scattering angle  $\theta$  at  $\lambda = 440$  nm and 620 nm, as obtained in 1983 (different polarimeter and telescope from 1988) and 1985 (same polarimeter and telescope as in 1988). Open circles are before inferior conjunction. Representative values of the standard deviation are indicated. The curves are the background polarizations of the 1988 runs (Figs. 7, 10).

behavior. This holds particularly for the present situation where the optical path through the atmosphere is at very low elevations. Temporal fluctuations in the spatial crystal density or preferential orientation and in the transparency of the atmospheric layers above the crystals may account for the observed large scatter in the points of anomalous polarization. Whenever spatial detail is present, its motion across terminator and limb, driven by the 4-day upper-atmospheric rotation, is another source of temporal modulation on a time scale of hours.

Temporal variation of the dips on a longer time scale is represented by the greater angular width of the 1988 I dip (observed on the other side of Venus with changed atmospheric conditions). As explanations one may invoke a changed transparency of the atmosphere combined with a vertical gradient in crystal contamination, or an increased broadening due to a smaller mean size of the scattering crystals in the way described by Eqs. (3) and (4). The gradient explanation fits best, since the observed

steep wing of the 1988 I dip contradicts the other explanation and the amplitude of the dip does not decrease as the dip broadens. At the 1988 I extension of the dip to  $\theta \cong 24.5^\circ$ , the halo angle for pure ice is exceeded by about  $3^\circ$  (Fig. 13), but a contamination of 28% weight percentage  $\text{H}_2\text{SO}_4$  (1 molecule  $\text{H}_2\text{SO}_4$  in 14 molecules ice) would explain such a shift in halo angle. Because of vaporization, more contamination may occur at the lower level of a crystal layer and an increased transparency could expose the more contaminated ice in the deeper atmospheric layers to a greater extent.

Since the broadening mechanism of Eqs. (3) and (4) has been ruled out as the main cause of the observed width of the dip, an exact value of the size of the scattering crystals cannot be determined. However, the largest observed width of about  $3^\circ$  (1988 I; 850 nm) and Eq. (4) put a lower limit of  $10 \mu\text{m}$  on the slitwidth  $a$ . Hence a halo interpretation of the dip requires a diameter of at least  $25 \mu\text{m}$  for the hexagonal crystal face.

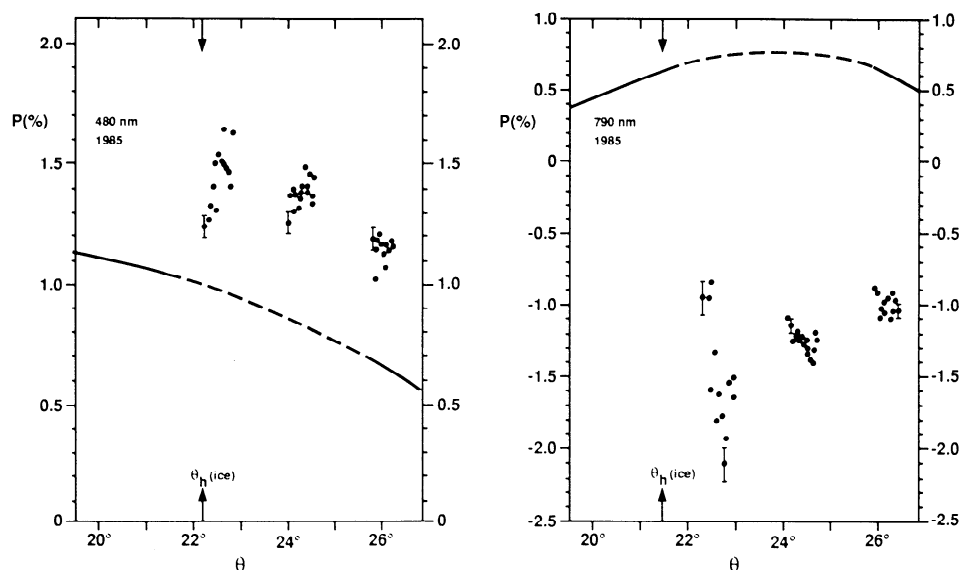


FIG. 15. Venus polarization  $P$  as a function of scattering angle  $\theta$  at  $\lambda = 480$  nm and 790 nm, obtained in 1985 (same polarimeter and telescope as in 1988). Representative values of the standard deviation are indicated. The anomalously large scatter in the points of the steep  $\lambda = 790$  nm dip near  $\theta = 23^\circ$  reflects rapid fluctuations of the Venus polarization signal. The curves are the background polarizations of the 1988 runs (Figs. 5, 9).

This raises the question from what atmospheric level the signal originates. As pointed out to us by A.T. Young (private communication), the effective scattering layer (optical depth of order unity) is located well over the main cloud tops for the large phase angles involved here. At  $\theta \approx 24^\circ$ , the optical path through the Venus atmosphere is at almost grazing incidence; in the equatorial region of the crescent, the air-mass factor is about 5. Both the UV and  $\text{CO}_2$  absorption, whose wavelengths bracket our observations, are about three times less than in the backward scattering configuration ( $\theta = 180^\circ$ ), so the air mass in the low-incidence  $\theta = 24^\circ$  light path is about three times less than in a back-scattered light path (Young 1977). In combination with the air-mass factor of 5 this implies that there is 15 times less air in the column above the effective scattering layer than in the case of  $\theta = 180^\circ$ , where we see the cloud tops at 65 km. This locates the layer at roughly 80 km, near the 170 K mesopause temperature minimum of the Venus atmosphere, in the region of the upper haze.

In the terrestrial mesosphere, the atmospheric pressure is not far from the saturation vapor pressure of ice, and therefore the mesospheric noctilucent clouds are only rarely formed. At Venus the much higher atmospheric pressure creates better conditions for crystallization in its mesosphere, provided that there is enough humidity. Nevertheless, the particle size both in the Venus upper haze and in its terrestrial analogue is believed to be in the submicrometer range (Kawabata *et al.* 1980, Knollenberg *et al.* 1980, Gadsden and Schröder 1989), which is two orders of magnitude lower than the size required in the halo interpretation. Like the terrestrial situation, the

Venus upper mesosphere seems to be characterized by an active circulation (Limaye 1984) with strong vertical motions, and the denser Venus atmosphere can lift much larger particles. It is an open question whether there is indeed a sufficiently long tail in the crystal size distribution in the equatorial upper haze.

There is a more serious flaw in the halo interpretation. Not only is the magnitude of the dip strongly wavelength-dependent, but this dependence contradicts that expected for a halo: a halo birefringence peak should be stronger at shorter rather than at longer wavelengths. Strongly colored crystals would save the interpretation, but it is difficult to understand why the crystals should be of a deep-red color.

In summary, the nature of the dip cannot be identified conclusively. Some of the properties of this recurring feature are consistent with a halo explanation, but the wavelength dependence is not. Intensity measurements would have provided a clue to the solution of this problem, since if the observed dip is a halo, it must be accompanied by an increase in Venus intensity of at least 4% at 850 nm (see Eq. (7)), but sufficiently accurate intensity measurements simultaneous with our polarization observations are lacking.

Even if the interpretation of the polarization anomaly as halo scattering is in the main correct, it explains only part of the observed features. At least one other mechanism is needed to explain the 1988 I peak at 622 and 712 nm. Since this peak showed up in one time series only, it seems to be a transient feature, either blocking or over-compensating the alleged halo dip; its nature remains a

matter of speculation. The measurements indicate that the time scale of this feature was somewhat smaller than that of the dips, since the 712-nm measurements of 1988 I suggest that the peak was followed by a very narrow dip at  $\theta \cong 24^\circ$ , possibly part of the otherwise obscured dip at that wavelength, showing up when the anomalous peak ceased.

Although the very nature of the time series excludes a unique explanation of all the observed features, and even the halo interpretation of the recurring dip is perhaps debatable, it is beyond doubt that noteworthy effects are happening in the Venus polarization, particularly at scattering angles near  $23\text{--}25^\circ$ . Full exploration requires evenly distributed time series without the gaps caused by the daily setting of Venus, information about the spatial distribution of the polarization, monitoring of the intensity at one of the spots on Venus selected for the polarization observations, and repetition of the measurements with a higher frequency than that of inferior conjunctions. Measurements from Earth can never meet all these requirements and in fact one would be unlikely even to repeat the quality of our 1988 II series, for which almost all circumstances were optimal. The only extension worth aiming for would be a time series of imaging polarimetry at say 600 and 800 nm, using several telescopes to close the gaps in the series, but even such a major campaign would solve only part of the interpretation problems. Substantial improvement requires a high-angular-resolution multiwavelength polarimeter on a Venus orbiter.

The present work used halo birefringence as diagnostic, a method unexplored so far. Our measurements of the polarization of terrestrial halos indicate the potential of the method, even for a weakly birefringent species like ice (Können and Tinbergen 1991, Können 1992). This opens intriguing possibilities for the detection of birefringent crystals floating in the atmospheres of other planets or their satellites (Whalley and McLaurin 1984) or perhaps located on their solid surfaces (see a picture of W. Tape, Plate 2-25 in Greenler 1980 for a terrestrial example). Solid nitrogen, the ammonia hydrates, and sulfur dioxide are among the species which may be detected by this method. As a halo birefringence peak can be very narrow, polarimetry of high angular resolution is required. This requirement becomes increasingly significant when the planet is far from the Sun and the birefringence is weak. For instance, for ice on Saturn or beyond, an angular resolution of better than  $0.05^\circ$  is required to resolve the halo anomaly completely. Since halo scattering is only visible from the far side of a planet, space probes will be needed for its detection.

## 7. CONCLUSIONS

Fluctuations in the Venus polarization are detected with time scales ranging from less than an hour to years. For

one type of fluctuation, characterized by a decreased polarization lasting 1 or 2 days but occurring only at long wavelengths, the most likely cause is Venus passing through a scattering angle range with decreased polarization. A possible explanation is halo scattering by  $\text{H}_2\text{SO}_4$ -contaminated ice crystals located in the Venus upper haze, but the wavelength dependence of the magnitude of the dip is difficult to understand and may argue for some other mechanism. Superposed on the dip there are rapid time fluctuations. As in the terrestrial situation, they seem to be caused by transient atmospheric phenomena like changes in the density in the cloud of scatterers or temporary blocking of the polarization anomaly due to movement of high-level atmospheric structures driven by the strong atmospheric circulation. Venus meteorology is also considered to be responsible for the fluctuating width of the dip. After weeks or years the state of the atmosphere has changed, and apart from that systematic differences may exist for Venus morning and evening conditions. A relatively small increase in the transparency above the atmospheric layer containing the polarizing scatterers will broaden a halo peak toward larger scattering angles whenever the degree of crystal contamination increases with depth.

The last type of short-term polarization fluctuation identified is attributed to a transient atmospheric feature. It was observed only once and showed up as 2 days of increased polarization at intermediate wavelengths. Perhaps by chance it occurred simultaneously with the proposed halo dip visible at the longer wavelengths. Repeated detection would be required to identify its physical nature.

Our observations show the potentials of halo polarimetry as a diagnostic for detecting birefringent crystals in planetary atmospheres. Because of the sensitivity of the method it does seem worthwhile to equip future outer planetary missions and Earth remote-sensing satellites with a polarimeter of high spatial resolution.

## ACKNOWLEDGMENTS

We thank R. E. Wallis and D. Hofstadt for their support during the La Palma and La Silla measurements, respectively, J. Meeus for providing the Venus coordinates long in advance, and A. Dollfus for his advice on polarimetry near the Sun. Sara Muller provided constructive comments and help on the data analyses. A. T. Young and J. W. Hovenier's comments on the interpretation of the data are gratefully acknowledged. The incisive comments by H. C. van de Hulst led to a substantially improved paper.

The Jacobus Kapteyn Telescope is operated by the Royal Greenwich Observatory at the Spanish Observatorio del Roque de los Muchachos of the Instituto de Astrofísica de Canarias on behalf of the Science and Engineering Research Council (SERC) of the United Kingdom and the Netherlands Organization for Scientific Research (NWO).

This work was financially supported by the Leids Kerkhoven-Bosscha Fonds, the Leids Sterrewacht Fonds, and by the Netherlands Organization for Scientific Research.

## REFERENCES

- BEHR, A. 1968. *ESO Bulletin*, No. 5.
- DOLLFUS, A., AND D. L. COFFEEN 1970. Polarization of Venus. I. Disk observations. *Astron. Astrophys.* **8**, 251–266.
- ESPOSITO, L. W., R. G. KNOLLENBERG, M. YA. MAROV, O. B. TOON, AND R. P. TURCO 1983. The clouds and hazes of Venus. In *Venus* (D. M. Hunten, L. Colin, T. M. Donahue, and V. I. Moroz, Eds.), Univ. of Arizona Press, Tucson, Arizona.
- GADSDEN, M., AND W. SCHRÖDER 1989. *Physics and Chemistry in Space*, Vol. 18, *Noctilucent Clouds*, Planetology, Springer, Berlin.
- GIAUQUE, W. F., E. W. HORNUNG, J. E. KUNZLER, AND T. R. RUBIN 1960. The thermodynamic properties of aqueous sulfuric acid solutions and hydrates from 15 to 300 K. *J. Am. Chem. Soc.* **82**, 62–70.
- GREENLER, R. 1980. *Rainbows, Halos and Glories*, Cambridge University Press, Cambridge, U.K.
- HANSEN, J. E., AND J. W. HOVENIER 1974. Interpretation of the polarization of Venus. *J. Atmos. Sci.* **31**, 1137–1160.
- HOBBS, P. V. 1974. *Ice Physics*, Clarendon Press, Oxford.
- HSU, J.-C., AND M. BREGER 1982. On standard polarized stars. *Astrophys. J.* **262**, 732–738.
- KAHANE, A. 1962. *Recherches expérimentales et théoriques sur les propriétés optiques et la structure de la glace*. Thesis, Université de Paris, faculté des sciences.
- KAWABATA, K., D. L. COFFEEN, J. E. HANSEN, W. A. LANE, M. SATO, AND L. D. TRAVIS 1980. Cloud and haze properties from Pioneer Venus polarimetry. *J. Geophys. Res. A.* **85**, 8129–8140.
- KNOLLENBERG, R. G., AND D. M. HUNTEN 1980. The microphysics of the clouds of Venus: Results of the Pioneer Particle Size Spectrometer experiment. *J. Geophys. Res. A.* **85**, 8039–8058.
- KNOLLENBERG, R., L. TRAVIS, M. TOMASKO, P. SMITH, B. RAGENT, L. ESPOSITO, D. MCCLEESE, J. MARTONCHIK, AND R. BEER 1980. The clouds of Venus: A synthesis report. *J. Geophys. Res. A.* **85**, 8059–8081.
- KÖNNEN, G. P. 1985. *Polarized Light in Nature*, Cambridge University Press, Cambridge U.K.
- KÖNNEN, G. P. 1992. Photopolarimetry of halos and ice crystal sizing. *Antarctic J. U.S.*, 1992 Review Issue, in press.
- KÖNNEN, G. P., AND J. TINBERGEN 1988. Venus, Meteorology and the Jacobus Kapteyn Telescope, *Gemini* **22**, 12–13.
- KÖNNEN, G. P., AND J. TINBERGEN 1991. Polarimetry of a 22° halo. *Appl. Opt.* **30**, 3382–3400.
- LIMAYE, S. S. 1984. Morphology and movements of polarization features on Venus as seen in the Pioneer Orbiter Cloud Photopolarimeter data. *Icarus* **57**, 362–385.
- LOMMEL, E. 1877. Bemerkungen über die Polarisation des Regenbogens. *Pogg. Ann. Physik* **160**, 147–150.
- MARTENS, F. F. 1906. Die Brechungsindizes. In *Handbuch der Physik* **6**, *Optik* (A. Winkelmann, Ed.), p. 649, Johann Barth, Leipzig.
- MINNAERT, M. 1954. *The Nature of Light and Color in the Open Air*. Dover N.Y.
- OHTAKE, T. 1993. Freezing points of H<sub>2</sub>SO<sub>4</sub> aqueous solutions and formation of stratospheric ice clouds. *Tellus*, in press.
- O'LEARY, B. T. 1966. The presence of ice in the Venus atmosphere as inferred from a halo effect. *Astrophys. J.* **146**, 754–766.
- O'LEARY, B. T. 1970. Venus halo: Photometric evidence for ice in the Venus clouds. *Icarus* **13**, 292–298.
- SEIFF, A. 1983. Thermal structure of the atmosphere of Venus. In *Venus* (D. M. Hunten, L. Colin, T. M. Donahue, and V. I. Moroz, Eds.), Univ. of Arizona Press, Tucson, Arizona.
- SEIFF, A., D. B. KIRK, R. E. YOUNG, R. C. BLANCHARD, J. T. FINDLAY, G. M. KELLY, AND S. C. SOMMER 1980. Measurements of thermal structure and thermal contrasts in the atmosphere of Venus and related dynamical observations: Results of the four Pioneer Venus probes. *J. Geophys. Res. A.* **85**, 7903–7933.
- TAPE, W. *Halos: Celestial Manifestations of Crystalline Beauty*, in preparation.
- TINBERGEN, J. 1979. A list of zero-polarization standards. *Astron. Astrophys. Suppl.* **35**, 325–326.
- UNGER, S. W., E. BRINKS, R. A. LAING, K. P. TRITTON, AND P. M. GRAY 1988. *Observers' Guide, Isaac Newton Group, La Palma*, pp. 149–151. Royal Greenwich Observatory, Cambridge, England.
- VEVERKA, J. 1971. A polarimetric search for a Venus halo during the 1969 inferior conjunction. *Icarus* **14**, 282–283.
- WARD, D., AND B. T. O'LEARY 1972. Search for a Venus halo effect during 1970. *Icarus* **16**, 314–317.
- WHALLEY, E., AND G. E. MCLAURIN 1984. Refraction halos in the solar system. I. Halos from cubic crystals that may occur in atmospheres in the solar system. *J. Opt. Soc. Am. A.* **1**, 1166–1170.
- YOUNG, A. T. 1973. Are the clouds of Venus sulfuric acid? *Icarus* **18**, 564–582.
- YOUNG, A. T. 1977. An improved Venus cloud model. *Icarus*, **32**, 1–26.